Integrating experimental and simulation length and time scales in mechanistic studies of friction

2008 J. Phys.: Condens. Matter 20 354012

(http://iopscience.iop.org/0953-8984/20/35/354012)

IOP Publishing Journal of Physics: Condensed Matter

J. Phys.: Condens. Matter **20** (2008) 354012 (14pp) doi:10.1088/0953-8984/20/35/354012

Integrating experimental and simulation length and time scales in mechanistic studies of friction

W G Sawyer[1,2], S S Perry[2], S R Phillpot[2] and S B Sinnott[2,3]

[1] Department of Mechanical and Aerospace Engineering, University of Florida, Gainesville, FL 32611, USA
[2] Department of Materials Science and Engineering, University of Florida, Gainesville, FL 32611, USA

E-mail: ssinn@mse.ufl.edu

Received 20 February 2008, in final form 18 April 2008
Published 11 August 2008
Online at stacks.iop.org/JPhysCM/20/354012

Abstract

Friction is ubiquitous in all aspects of everyday life and has consequently been under study for centuries. Classical theories of friction have been developed and used to successfully solve numerous tribological problems. However, modern applications that involve advanced materials operating under extreme environments can lead to situations where classical theories of friction are insufficient to describe the physical responses of sliding interfaces. Here, we review integrated experimental and computational studies of atomic-scale friction and wear at solid–solid interfaces across length and time scales. The influence of structural orientation in the case of carbon nanotube bundles, and molecular orientation in the case of polymer films of polytetrafluoroethylene and polyethylene, on friction and wear are discussed. In addition, while friction in solids is generally considered to be athermal, under certain conditions thermally activated friction is observed for polymers, carbon nanotubes and graphite. The conditions under which these transitions occur, and their proposed origins, are discussed. Lastly, a discussion of future directions is presented.

(Some figures in this article are in colour only in the electronic version)

1. Introduction

Friction is a ubiquitous phenomenon, occurring in virtually every aspect of life on a daily basis. It has consequently been under study for the last five centuries. Classical theories of friction have been developed that have been successfully applied to numerous tribological problems associated with contemporary life [1–4]. However, modern applications that involve solid–solid interfaces and advanced materials operating under extreme environments can lead to situations where classical theories are insufficient to describe friction at sliding interfaces. A concerted effort has therefore been made to link cutting edge experimental and computational work across length and time scales to develop new theories to characterize the frictional properties of solid–solid interfaces.

The study of atomic- and molecular-scale friction has been facilitated by experimental techniques developed and optimized over recent years, such as the atomic force microscope (AFM). The application of AFM to the study of friction provides the opportunity to probe tribological events under a number of desirable conditions. First, due to the inherent sharpness of the probe tip employed in AFM, this approach allows the investigation of single point contacts, essentially modeling the interaction of an individual asperity. Second, with the selection of appropriate cantilever force constants and operation at appropriate force (pressure) regimes, AFM studies provide access to measurements of interfacial friction in the absence of concurrent wear. Finally, the length scale of the microscopic approach provides data directly related to discreet atomic or molecular events, i.e. stick–slip motion of a probe tip laterally translated on a crystalline surface. However, it must also be acknowledged that AFM approaches face a number of challenges, potentially impacting the physical measurement as well as the interpretation of the data. These

[3] Author to whom any correspondence should be addressed.

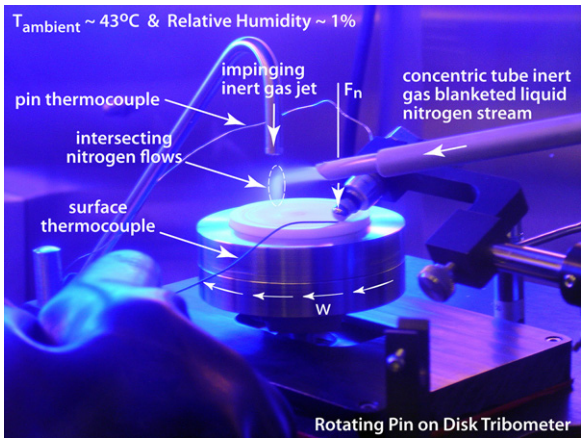

Figure 1. Photograph of the pin-on-disk microtribometer operating in a controlled atmosphere within a humidity controlled glove box that contains pure dry nitrogen gas. The impinging inert gas jet and intersecting nitrogen gas flows are indicated in the figure.

include the inability to directly determine the composition of the probe tip and the uncertainties associated with force measurements conducted with a microscopic cantilever spring system. Nonetheless, AFM measurements have significantly contributed to the body of fundamental knowledge of materials friction interactions [5].

The study of friction has also been enhanced by advancements to traditional experimental methods, such as the linear reciprocating tribometer. These advancements include the ability to vary and stabilize temperature over a wide range (from 190 to 450 K), and to modify and control of atmospheric conditions during tribological experiments. For example, figure 1 depicts the rotating pin-on-disk tribometer and nitrogen gas lines used to study friction at cryogenic temperatures. Such controls have led to much greater control of experimental uncertainties and thus to greater precision in the experimental measurements [6]. Taken together, these instrumental developments and the enabled measurements have provided new insights into friction.

Atomic- and molecular-scale details of friction have also been revealed through advances in computational methods and by the rapid rise in computer power over the last few years. Classical molecular dynamics (MD) simulations are of particular importance, as they allow the explicit determination of trajectories for every atom in the system as a function of time. MD involves the numerical integration of the Newtonian equations of motion:

$$\mathbf{F} = m\mathbf{a}, \tag{1a}$$

or equivalently,

$$-\nabla E = m(\mathrm{d}^2\mathbf{r}/\mathrm{d}t^2). \tag{1b}$$

Here, **F** is the (vector) force that acts on each atom, which is the gradient of the potential energy (E) felt by each atom; m is the atomic mass, **a** is the acceleration of each atom, **r** is the position of each atom, and t is time.

In the simulations described in this review, the forces are calculated using the second generation reactive empirical bond order (REBO) potential [7, 8]. The form of the potential is:

$$E = \sum_i \sum_{j(>i)} [V_{\mathrm{R}}(r_{ij}) - b_{ij} V_{\mathrm{A}}(r_{ij})] \tag{2}$$

where $V_{\mathrm{R}}(r)$ and $V_{\mathrm{A}}(r)$ are pair-additive interactions that model the interatomic repulsion and electron–nuclear attraction, respectively, r_{ij} is the distance between nearest-neighbor atoms i and j, and b_{ij} is a bond order term that takes into account the many-body interactions between atoms i and j, including those due to other nearest neighbors and due to bond bending effects. The potential is short ranged and only considers nearest neighbor, covalent interactions. Therefore, long-range interactions are modeled by coupling [9] the REBO potential to a Lennard-Jones (LJ) potential [10].

The REBO potential does a good job of describing the bonding in carbon-based materials, including diamond [11–13], amorphous carbon [14, 15], carbon nanotubes [16, 17], self-assembled monolayers [18–20], organic molecules [21, 22], and polymers [22, 23]. However, the REBO potential does not explicitly include electronic or quantum effects, which limits its inherent accuracy. Nonetheless, in cases where explicit comparisons have been made to more accurate approaches, this potential has been shown to give suitably accurate results for it to be used in the studies reported below with confidence [24].

The application of these experimental and computational methods to understanding the effect of molecular orientation and temperature on the frictional properties of solid–solid interfaces is addressed in the next two sections. This is followed by some general conclusions and a discussion of future directions.

2. Orientation effects on friction

2.1. Carbon nanotube systems

Carbon nanotubes (CNTs) have high tensile and flexural strengths, high elastic moduli, high aspect ratios, and low densities [25]. These properties make them attractive for use in applications where friction is important, such as nanoelectromechanical systems (NEMS) [26] and composites [27]. The fact that films of CNTs may be readily deposited by chemical vapor deposition enhances their potential use as tribological films. Here we review recent experimental and computational findings regarding the tribological properties of individual carbon nanotubes and nanotube films.

Previously, the tribological properties of individual nanotubes were examined using AFM [28, 29] and MD simulation [30]. The motion of the nanotubes (rolling versus sliding) was determined by the registry of the CNT with the underlying graphite surface. When the hexagonal pattern of the CNT aligned with the hexagonal pattern of the graphite, the CNT rolled. On the other hand, when these hexagonal lattices were out of registry, the CNT slid in response to applied forces.

The tribological properties of films of CNTs were examined computationally prior to experimental investigations because of the availability of realistic potentials [7] and the ability of simulations to avoid the difficulties inherent

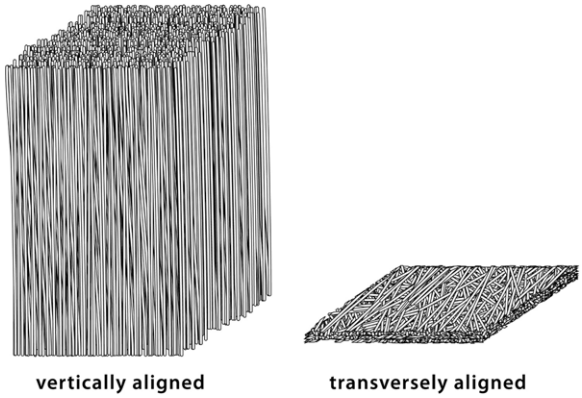

Figure 2. Schematic of vertically aligned and transversely aligned carbon nanotube films.

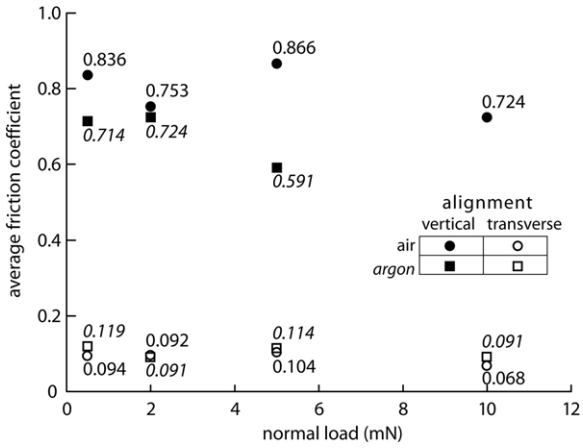

Figure 3. The average friction coefficient of chemical vapor deposition grown multi-walled CNTs as a function of orientation in air and argon environments.

in synthesizing and manipulating these nanometer-scale structures. In particular, MD simulations [31] predicted that the responses of bundles of single-walled CNTs subjected to compressive and shearing forces between two diamond surfaces varied depending on their orientation (see figure 2). Bundles that were oriented horizontally to the sliding surfaces exhibited sliding, and mixed sliding and rolling motions, while vertically aligned CNT bundles buckled in response to compression, and leaned in the direction of sliding. Vertically aligned bundles had higher friction coefficients than horizontally aligned bundles.

These predictions have subsequently been confirmed in experiments [32], in which highly anisotropic tribological properties were observed to depend on the orientation of the multi-walled CNT films relative to the sliding surfaces, in good agreement with the computational predictions, as indicated in figure 3. In particular, the average experimental friction coefficients of the CNT films ranged from high values of 0.795 for vertically aligned nanotubes, to quite low values of 0.090 for nanotubes that were oriented transversely on the surface. These frictional properties were not sensitive to changes in humidity.

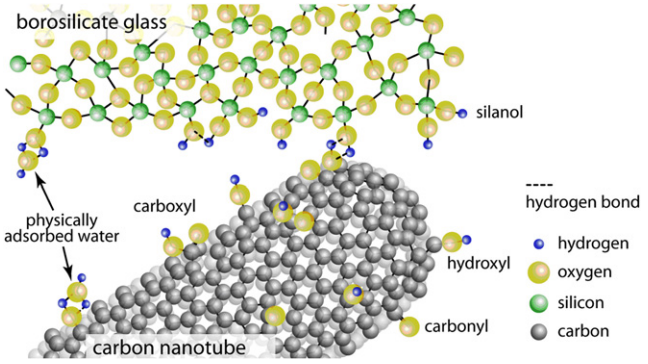

Figure 4. Schematic of the molecular interactions between CNTs and borosilicate glass during sliding that are inferred from the experiments.

More recent experiments on multi-walled CNTs [33] found that their frictional properties changed significantly as a function of surface chemistry between the CNTs and the sliding counter surface of either glass or gold-coated glass, as illustrated in figure 4. The CNTs were cleaned by oxygen plasma etching, which removed excess soot and amorphous carbon and chemically modified the CNT walls with carboxyl and carbonyl groups. These groups formed hydrogen bonds with the silica glass, which ultimately dominated the frictional responses of the CNT–glass system. However, this effect did not occur when the glass was coated with gold. In both cases, atmospheric water did not influence the results, which was attributed to the fact that the glass surface was fully saturated with water regardless of the level of humidity in the atmosphere.

Simulations [34] were also used to examine the effect of altering the structure of horizontally aligned bundles of CNTs from single-walled, to peapods (single-walled tubes filled with C_{60} molecules [35]), to double-walled multi-walled CNTs (single-walled tubes filled with other nanotubes). These bundles were placed between sliding diamond-like carbon surfaces. The results indicate that the filled CNT bundles can sustain higher compressive forces than the hollow CNT bundles. However, the filled CNT bundle has a similar friction coefficient to the hollow CNT bundles during sliding at low compressive pressures (see figure 5).

Recently, the effect of molecular fluids on CNT tribological responses was also evaluated in MD simulations [34]. The simulations predicted that the presence of the benzene molecules does not alter the rolling motions of the single-walled CNT and peapod bundles. However, the molecules readily slide over each other, which lowered the lateral forces for the CNT/benzene system. At the same time, the presence of the molecules causes greater misalignments among the CNTs in the bundle, which increased the lateral forces. The combination of these two effects canceled each other out and was the main reason that the ratio of the lateral and normal forces did not change much on the introduction of benzene molecules. This result differs from experimental data that indicated that the introduction of benzene molecules (see figure 5) on graphite surfaces decreased the friction coefficient

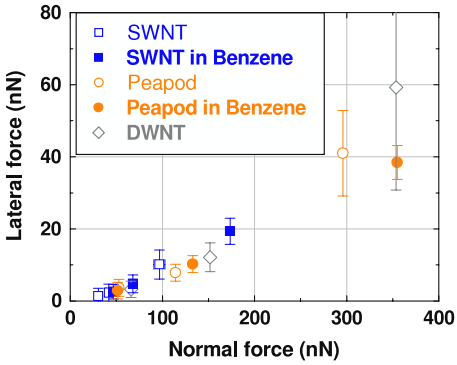

Figure 5. Lateral force versus normal force for single-walled nanotubes (SWNTs) in bare bundles or bundles surrounded by benzene, peapods that consist of SWNTs filled with C_{60} molecules in bare bundles or surrounded by benzene, and double-walled nanotubes (DWNTs). The values are predicted from MD simulations.

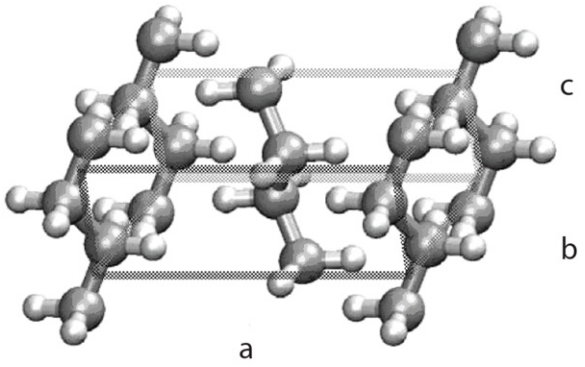

Figure 6. Schematic of the orthorhombic unit cells of PTFE and PE. For both polymers, the chain backbone is made of carbon atoms; the side groups are H for PE, and F for PTFE. For PTFE: $a = 0.873$ nm, $b = 0.569$ nm, $c = 0.262$ nm. For PE: $a = 0.741$ nm, $b = 0.494$ nm, $c = 0.254$ nm.

of graphite [36, 37]. This contradiction suggests that the influence of benzene on different systems fundamentally changes as a function of the curvature of the graphene sheets.

In summary, the experiments and simulations described above have demonstrated unequivocally that the orientation of carbon nanotubes within coatings strongly influences their tribological responses.

2.2. *Polymer systems*

The chemical inertness, high melting point, and intrinsic lubricity of polytetrafluoroethylene (PTFE) have been exploited for the development of solid lubricating parts for operation in extreme environments, in applications ranging from frying pans to satellites. Likewise, polyethylene (PE) is one of the most widely used polymers because of its versatility and manufacturability. It exhibits outstanding wear resistance and toughness, and has favorable tribological properties [38].

Although there is considerable evidence in the literature that molecular-scale interactions may dominate the observed macroscale friction response of PE and PTFE tribo-systems [39–45], there have been no molecular-scale investigations to substantiate this hypothesis. In studies of friction for various thermoplastics, Pooley and Tabor hypothesized that the molecular shape of the PTFE is responsible for its low friction coefficients [40]; furthermore, results from McLaren and Tabor suggest that adhesion processes are dominated by molecular-scale interactions rather than by asperity-scale interactions [46]. Discussions on the intrinsic lubricity of PTFE have proposed that the disruption of van der Waals interactions between adjacent PTFE molecules are responsible for the friction forces [47].

As Makinson and Tabor discovered [39], thin films of PTFE readily transfer to mating counterfaces, thus producing self-mated tribological contacts in almost all instances where this material is employed. It has been observed that these transfer films are oriented in the direction of sliding, but the extent of this orientation and its impact on the PTFE tribo-system is not known. Using grazing incidence x-ray diffraction, Breiby *et al* [48] found that the near surface region of the PTFE sample was aligned by the sliding action with a full width half maximum (FWHM) angular spread of ∼15°. The alignment of the thin transfer film however, was found to be substantially greater with a FWHM angular spread of only ∼0.23°. It was proposed that this high degree of molecular alignment within the sliding plane results in low friction by providing high stiffness normal to the sliding interface and low resistance to sliding along the molecular backbone.

Here we review recent findings, both experimental and from simulation, on the atomic-level mechanisms associated with tribology at PE and PTFE surfaces. In its highly crystalline state at ambient pressure and temperature, PE maintains an orthorhombic structure in which the carbon atoms along the chain axis are arranged in a planar zig-zag configuration, which is illustrated in figure 6. PTFE exhibits a similar crystal structure with different lattice parameters, albeit at high pressures that are consistent with those achieved in MD simulations of friction. These are the structures used in a number of studies using MD simulations to investigate the way in which inherent structural anisotropy of polymeric systems can lead to corresponding anisotropies in the tribological behavior, or, conversely, the way in which tribology can induce anisotropy in polymeric systems [49, 50].

Model transfer films of PTFE were deposited onto a thin steel foil, as shown schematically in figure 7. After creation, the foil-supported transfer films were cut into rectangular samples for testing. Custom designed sample mounts fixed opposing foils into a crossed-cylinder geometry. This geometry reduced misalignment sensitivity, minimized edge effects, and helped to reduce pressures to values more typical of those found in macroscale testing.

Normal and friction forces were continuously measured at the stationary foil, while the counterface underwent reciprocating displacement. Tests with an average sliding speed of 100 μm s^{-1} and a normal load of 500 mN were conducted over 250 sliding cycles. The friction and wear properties of the films themselves were measured using microtribometry; the results are shown in figure 8. We see from the friction loops that the parallel configuration displays a low friction coefficient before wearing through, while the

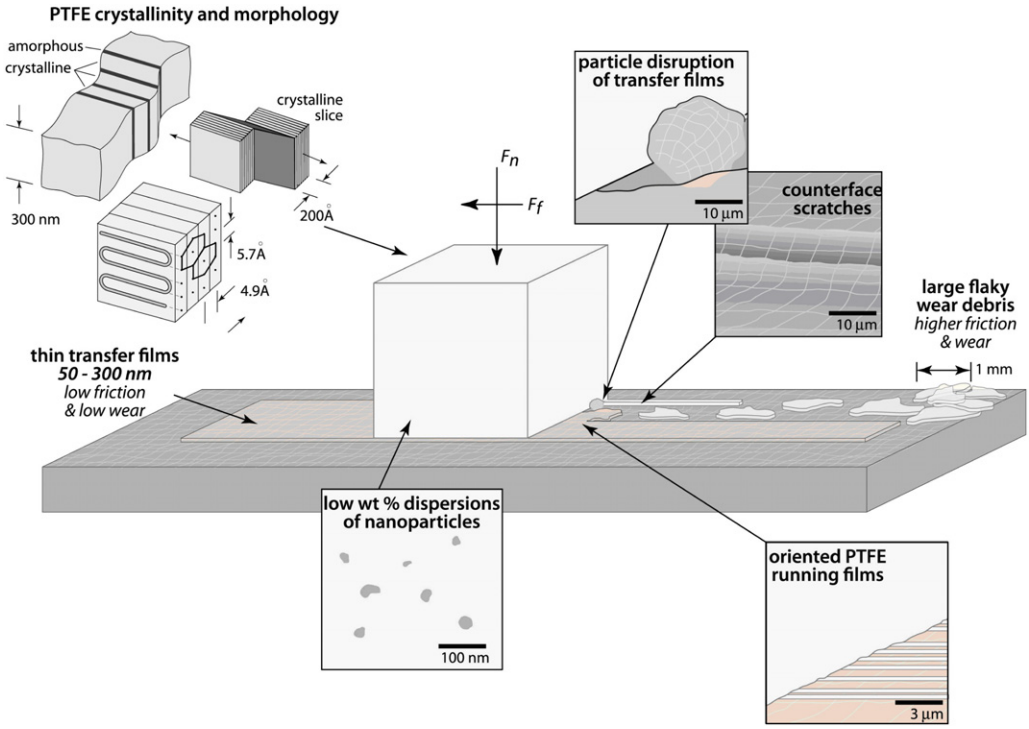

Figure 7. Schematic of the creation of PTFE running films in the pin-on-disk tribometer experiments.

perpendicular configuration exhibits a high and rapidly varying friction coefficient within the first few cycles. In addition, the measurements reveal that the parallel configuration is more than an order of magnitude more wear resistant than the perpendicular configuration, consistent with the MD simulation findings of interfacial sliding discussed below. Both the scatter and magnitude of friction for perpendicular sliding is attributed to molecular rearrangement within the cross aligned transfer films leading to film damage.

In order to visualize the nature of film alignment, PTFE transfer films were prepared through unidirectional sliding for AFM characterization. The transfer films were imaged using with an Asylum MFP-3D atomic force microscope, employing an AC imaging mode. The intermittent contact between the tip and sample in this mode significantly improved the spatial resolution and reduced material transfer to the tip from the PTFE samples. Similar features (film orientation) were observed in AFM images measured for continuous tip–sample contact, although with lesser resolution. Figure 9(a) shows a topographic image obtained through intermittent contact of a PTFE film generated by the procedures described above. At the highest spatial resolution obtained, a clear orientation of material at the PTFE surface is evident with molecular-scale features aligned with the sliding direction. Images obtained at lesser spatial resolution (data not shown) provided similar evidence of alignment in the sliding direction, however through the presence of oriented features of greater widths (∼100 nm). Figure 9(b) displays the relative cross sectional height of the features observed in figure 9(a). These molecular-scale measurements of order and orientation confirm the relevance of the simulations of oriented PTFE transfer films.

The sliding process was also modeled with classical atomic-scale MD simulations. The simulated polymer morphology (identical for PE and PTFE) is shown in figure 10. The system consisted of two crystals, with the polymer backbones in the two crystals being parallel to each other: full details of the simulation conditions are given elsewhere [51, 34]. As illustrated in figure 10, we considered two different sliding scenarios: sliding along a direction transverse to the chain axis is defined as perpendicular sliding, while sliding along the chain axis is defined as parallel sliding.

The simulations predicted that the overall sliding behaviors in the parallel and perpendicular directions are quantitatively and qualitatively different from each other, and suggested atomic-level mechanisms responsible for these differences. The normal and lateral forces (relative to the sliding direction and computed on the rigid moving layer of atoms) are shown in figure 11. During sliding in both orientations, the PTFE chains underwent structural changes, resulting in initial reductions in the normal forces. Interestingly, the frictional forces across the interface remained steady. In contrast, for perpendicular sliding there was an increase in normal force; again the frictional force remained approximately constant.

If the ratio of the lateral to normal force is taken, the value is an order of magnitude higher in the case of the perpendicular configuration compared to the parallel configuration. In a fist-order interpretation, this ratio may be identified with the friction coefficient through Amonton's friction equation ($F_N = \mu F_L$, where μ is the friction coefficient, F_L is the lateral force, and F_N is the normal or compressive force) [3]. This model is widely used to report relative values of friction in a way that is independent of normal load. However, the friction force

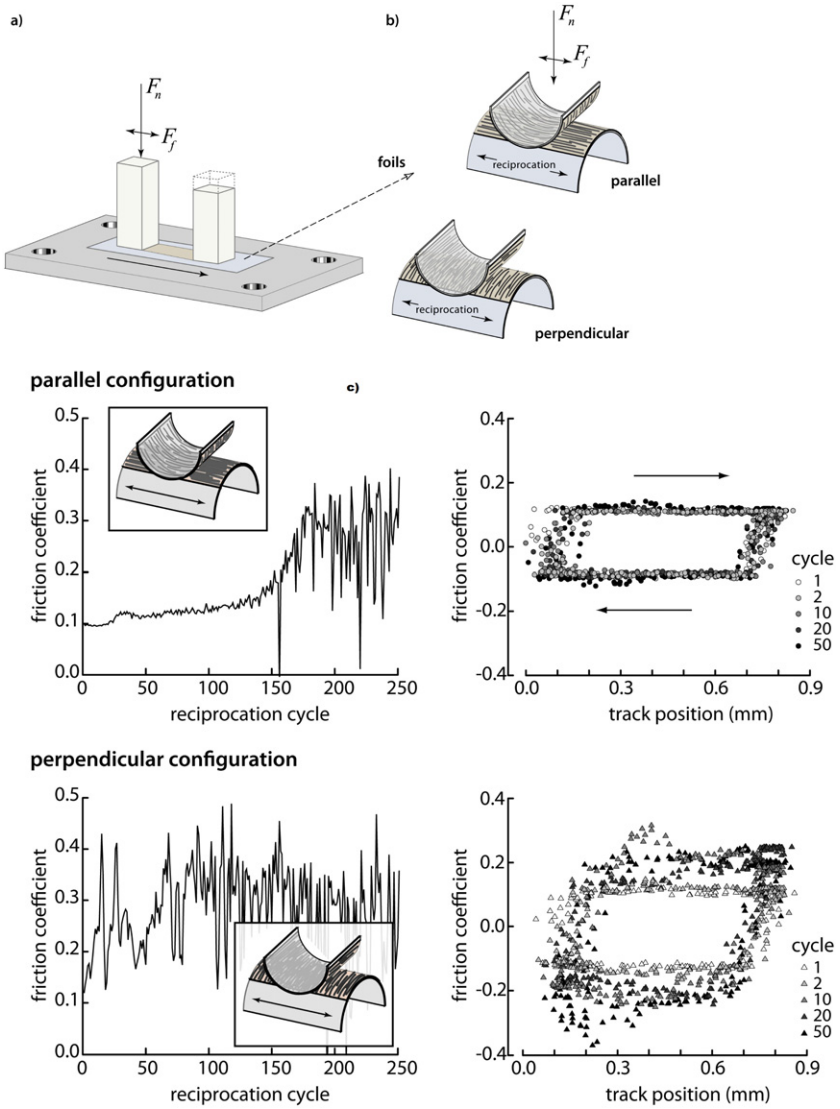

Figure 8. Microtribometry friction results (a) for the crossed-cylinder foils with oriented PTFE transfer films in different orientations (b). The friction coefficients are displayed versus reciprocation cycle in (c) for parallel and transverse or perpendicular configurations. The evolution of friction coefficient along the reciprocation track is also plotted for both the parallel and perpendicular configurations. The perpendicular alignment of the films leads to rapid failure of the films and high friction forces during the first 10 reciprocating cycles, whereas over 150 cycles are needed to realize similar levels in the parallel configuration. The low coefficient of friction for parallel sliding is consistent with the behavior of bulk PTFE samples; the transition to higher coefficients of friction is consistent with the film thickness and a wear rate of 10^{-5} mm^3 N m^{-1}.

is not universally independent of normal load. For example, non-linear force area relationships in contact often exhibit non-linear friction behavior. The additive effects of adhesion on contact pressures can be substantial if not dominant at the nano-scale. Efforts to report friction coefficients that are independent of load, area, and adhesive contributions to contact use a load-ramp technique. Thus, it is necessary to perform simulations over a range of normal forces. Figure 12 shows the results for one such set of load ramps. The slope of the linear fit to the F_N versus F_L fit is the true best estimate of the friction coefficient; the intercept on the F_L axis gives the adhesion force. The friction coefficient predicted in this manner for PTFE in the parallel configuration is 0.18, which is in excellent agreement with the experimentally determined value of about 0.13 (see figure 8).

The simulations can provide atomic-level mechanistic information that is not available experimentally. Figure 13 shows a series of images of the top 25 chains from the bottom PTFE surface. It is apparent from these images that the aligned structure of the PTFE is retained in the parallel sliding configuration over 40 nm of sliding (lower right). Analysis of the displacements of the uppermost row of carbon atoms with respect to their original position revealed that the chains in the parallel configuration were displaced during sliding relative to their original location by a maximum of ∼2.5% (∼1 nm over 40 nm) of the sliding distance, indicative of almost complete interfacial slip. In sharp contrast, for the case of perpendicular sliding, the images in figure 13 show that the alignment of the chains becomes progressively less well defined during sliding. In particular the highlighted chains that were previously on

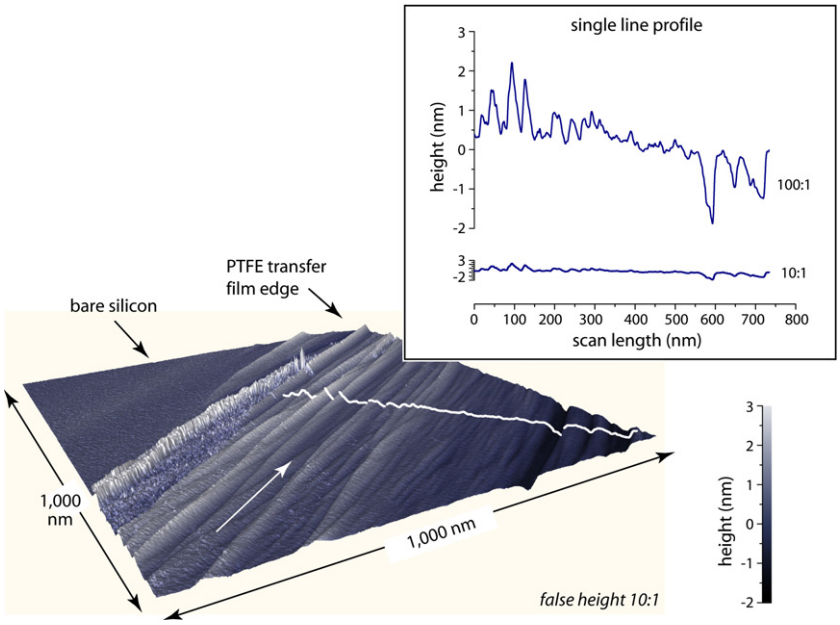

Figure 9. An intermittent contact AFM image of the transfer film produced through reciprocal sliding of PTFE on a polished steel substrate. The observed oriented features are highly correlated with the direction of sliding during the generation of the PTFE transfer film. The single line profile orthogonal to the sliding direction (inset) portrays surface features on the order of 10 nm in width and 2–3 nm in height; such features within the image strongly suggest the fibrillated and oriented nature of the transfer film.

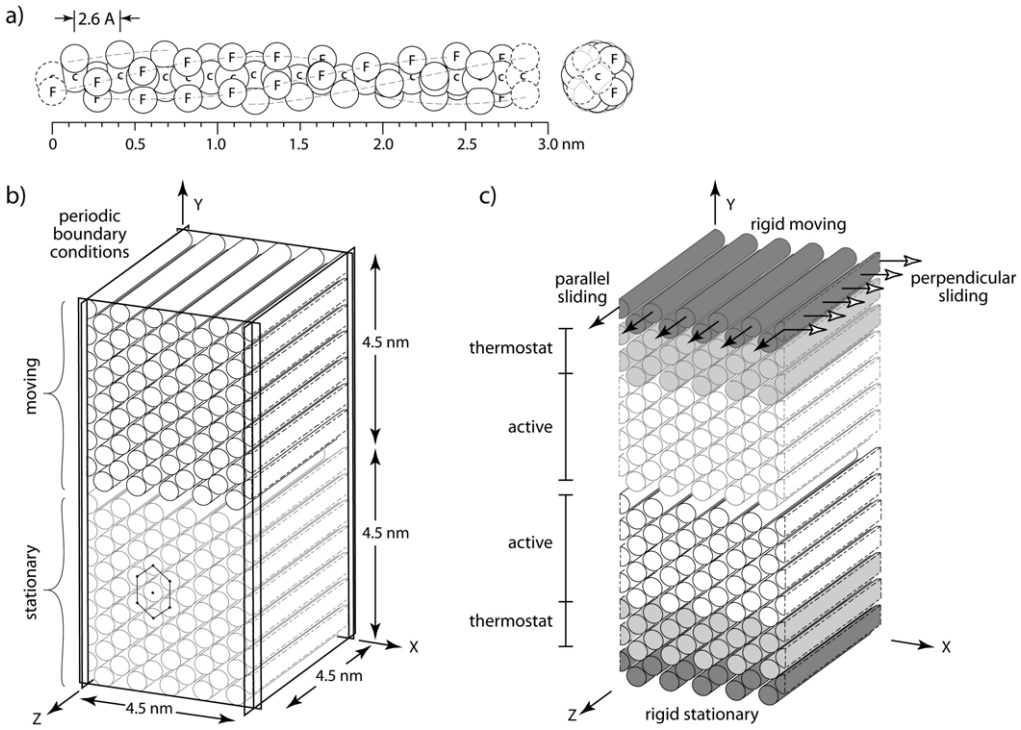

Figure 10. Schematic of the molecular dynamics simulations. (a) The repeating structure of PTFE is helical with repeating CF_2 units. (b) The atomistic simulation is periodic on the x and z faces. The simulation cell is comprised of two cross-linked aligned films of PTFE or PE. The hexagonal structure of the PTFE crystal is illustrated along with the dimensions of the simulation. (c) The simulation is comprised of opposing regions of rigid atoms, thermostated atoms, and active atoms of layer thickness 0.4, 0.8, and 2.4 nm, respectively, for PTFE, and 0.5, 0.5, and 2.4 nm, respectively, for PE. After equilibration, the upper block of rigid atoms are moved in the z direction (parallel) or the x direction (perpendicular), where parallel and perpendicular refer to the sliding direction relative to the chain alignment.

the top surface become mixed into the bulk. This mixing and deformation was dilatant, resulting in an increased normal force. Additionally, in the top views of the carbon atoms along the backbone of the top chains 1–5, chain scission is visible. Moreover, one of the broken chains aligns with the sliding direction. This structural reorganization is characteristic of

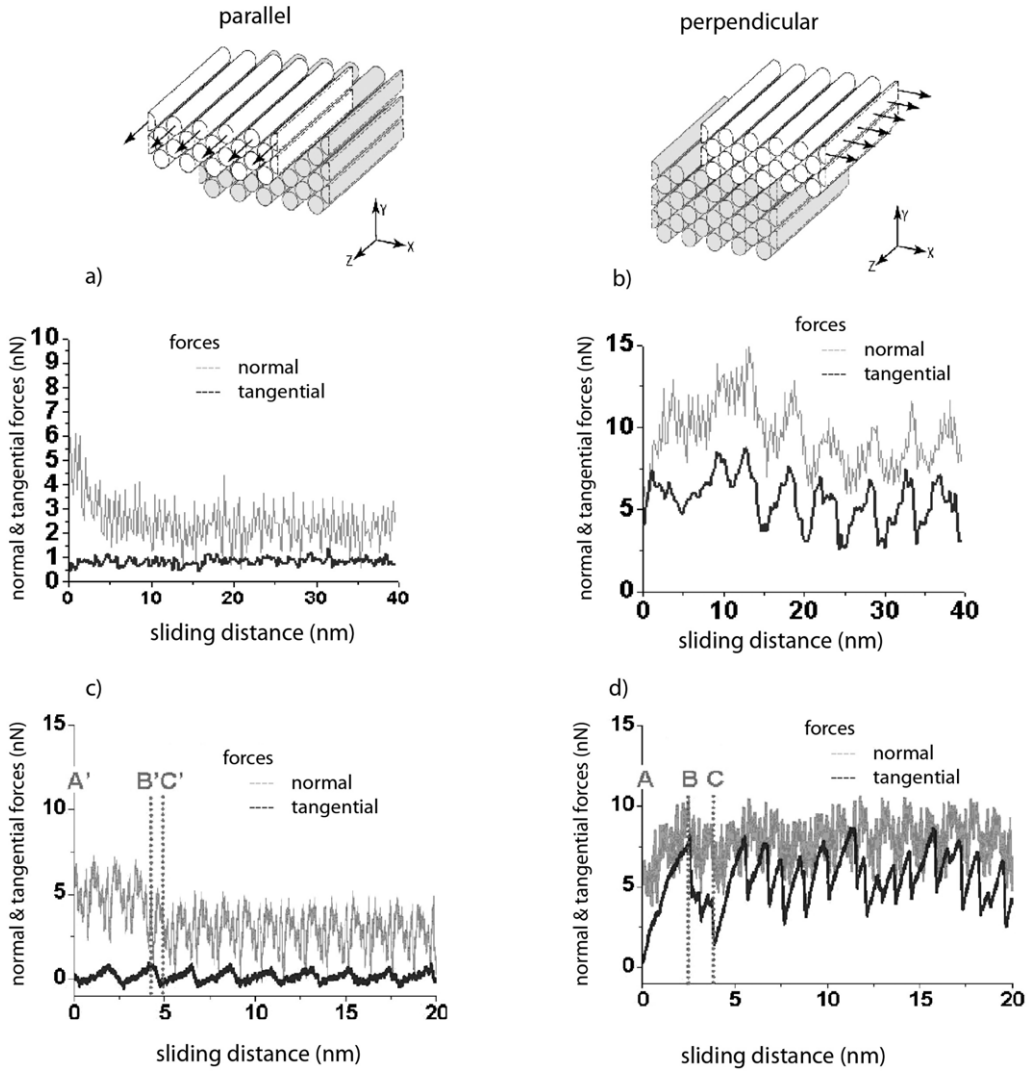

Figure 11. Normal and tangential forces for (a) PTFE in the parallel orientation, (b) PTFE in the perpendicular orientation, (c) PE in the parallel orientation, and (d) PE in the perpendicular orientation. In each case, the top and bottom polymer surfaces are compressed to a load of 5 nN before sliding is initiated. For parallel sliding (on the left), the average normal force decays with sliding distance due to the relaxation of compressive stresses, whereas the lateral forces remain low and steady. For perpendicular sliding (on the right), an increase in average normal force is observed due to dilation of the system with sliding. In (c) and (d), A′ and A represent the start of the simulation, B′ and B represent the point where relaxation and dilation is complete, and C′ and C represent the point at which the forces are recorded.

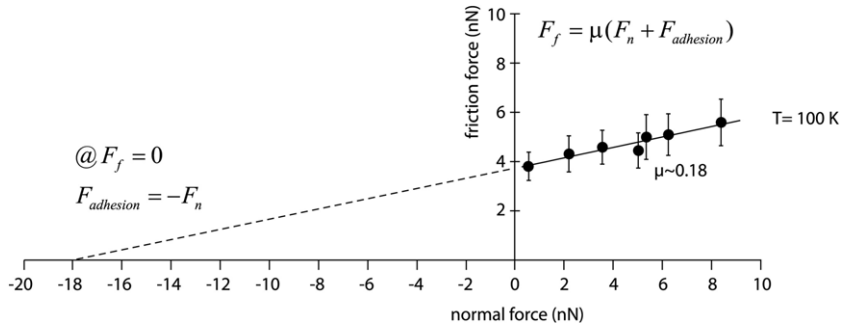

Figure 12. The dependence of the friction force on the normal force allows the friction coefficient and adhesive force to be determined. The non-zero adhesion force in these 100 K data for PTFE represent a violation of Amonton's law.

microscopic wear. We anticipate that further sliding would lead to further chain scissions, chain alignments and wear.

To assess how the molecular structure and stiffness of the polymer influences these responses, we compared the results for PTFE with those for PE. The trends in the normal and lateral forces with sliding distance were similar for both of these polymers, with the major difference being that the PE system exhibits stick–slip motion during both perpendicular

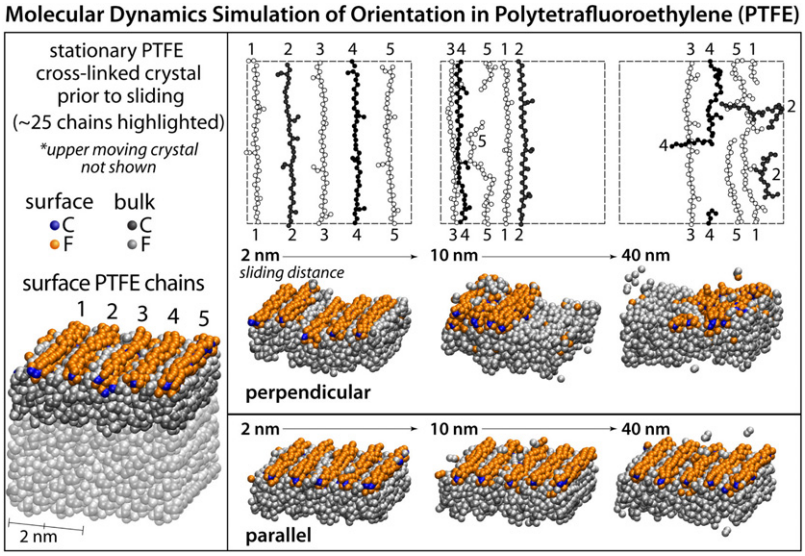

Figure 13. A sequence of snapshots of the upper 25 PTFE chains from the lower stationary PTFE crystal (left). The five surface chains are highlighted with blue (carbon) and orange (fluorine) atoms. The structure and alignment of these chains appears to be intact for the parallel sliding configuration (bottom), whereas the perpendicular sliding configuration produces gross chain motions and mixing within the highlighted region. The snapshots are taken at approximately 2, 10, and 40 nm of sliding. The top view of the carbon atoms for the five surface chains are shown at the same times for perpendicular sliding. Chain scission and realignment in the sliding direction is apparent in the 40 nm view.

and parallel sliding, while the PTFE system does not exhibit stick–slip motion (see figure 11). These different sliding behaviors are related to the nature of molecular motion. The bonds in the PE system are stiffer than in PTFE; consequently, a significantly higher degree of bond scission is observed in the case of either sliding configuration for PTFE compared to what is predicted to occur for PE. Such bond scission in the PTFE system represents a form of molecular-scale wear and gives rise to the mobility of a collection of molecules within the sliding interface that is not observed in the PE system. In turn, this molecular mobility acts to more evenly dissipate energy within the sliding interface, effectively eliminating the appearance of stick–slip behavior.

The data from these computational and experimental approaches, spanning length scales from the nanometers to centimeters, and time scales from nanoseconds to seconds, provide a consistent, atomic-level description of the mechanisms by which the structural orientation of PTFE contributes to its unique tribological properties.

The experiments and simulations described above have demonstrated unequivocally that molecular structural orientation at the sliding interfaces of PTFE and PE strongly influences friction and wear. For sliding of oriented chains parallel to the chain backbone, low friction forces and low barriers to interfacial slip are found. For sliding of oriented chains perpendicular to the chain backbones, friction and high wear in the form of molecular reorientation and scission are encountered. In the corresponding experiments, slow speed testing of bulk PTFE produces oriented transfer films similar to those examined in the simulations, as evidenced by molecular-scale AFM images. Microtribological measurements on these aligned films demonstrated a strong anisotropy in friction and wear, consistent with the molecular dynamics simulations.

3. Temperature effects

3.1. Polymers systems

Understanding the dependence of friction on temperature is critically important for numerous applications. For example, it is known that the viscosity of liquid lubricants increases as temperature decreases, thus producing related effects in the frictional properties of the liquid-lubricated system. The frictional properties of these systems will ultimately be a balance of the effects of reduced shear force and concomitant shear thinning. As systems operate in low temperature extremes, such as are present at high altitudes and in outer space, the use of liquid lubricants becomes impractical and solid lubricants are needed. Polymers and polymer composites have been demonstrated to be excellent solid lubricants for aerospace applications [52]. Friction, according to the classical Amonton's friction equation [3] is athermal. However, in the early 1970s Pooley and Tabor [40] discussed the thermal activation of friction in polymers such as PTFE; unfortunately, at this time definitive proof of athermal behavior was not available.

Recent analyses by McCook *et al* [47] and Burris and Sawyer [53] of that original data, and previous literature data from macroscopic experiments, showed that under non-wearing conditions the coefficient of friction of PTFE films and composites can be fit to an Arrhenius equation with an activation energy of about 3.7 kJ mol^{-1} over the temperature range of ~180–420 K (see figure 14). This activation energy is consistent with thermally activated breaking of van der Waals bonds between the sliding surfaces. This interpretation has been further supported by pin-on-disk studies of systems [33, 54, 55] for which only van der Waals interactions between the sliding surfaces were present.

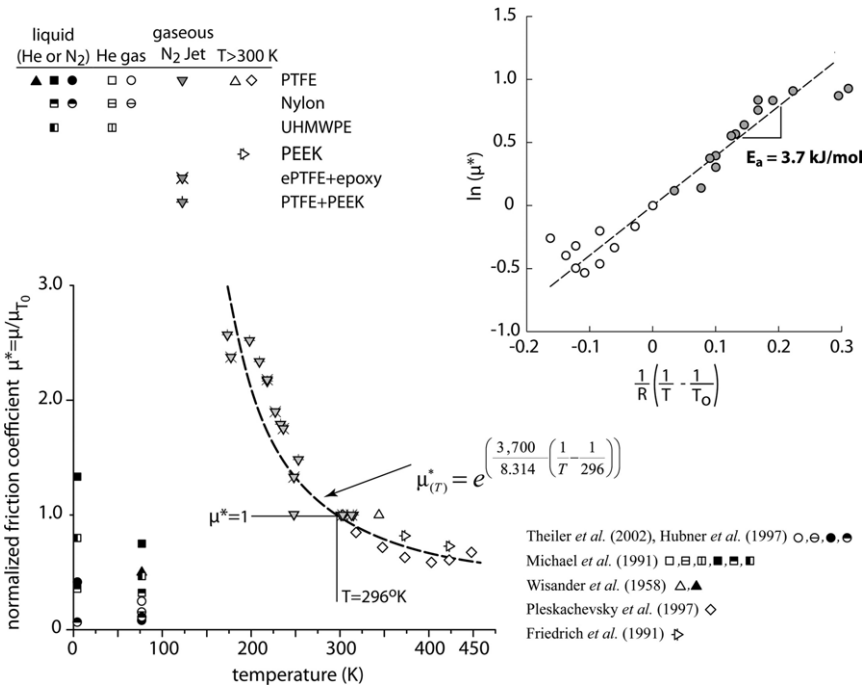

Figure 14. Normalized friction coefficients versus sample temperatures for a variety of polymers. If the data is from samples immersed in liquid nitrogen or helium, the symbols are filled in. The data is from [47] and references therein.

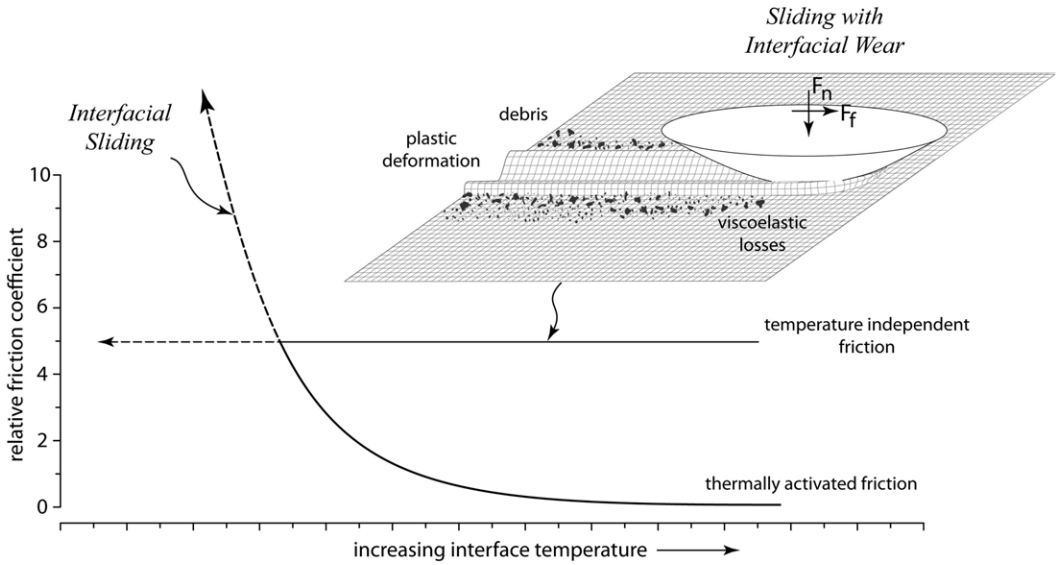

Figure 15. Schematic that illustrates the proposed hypothesis for the observed thermally activated friction that is observed in macroscale tribological experiments for materials where slip is accommodated through interfacial sliding.

Importantly, however substantially higher activation energies were obtained in systems with stronger interactions, such as hydrogen bonding [33] or hindered rotations of side groups [56]. Most interestingly, when the hydrogen-bonded material was coated with a thin layer of gold, the activation energy decreased to a value consistent with that of van der Waals interactions.

Figure 15 illustrates a possible hypothesis which entails thermally activated behavior in macroscopic tribology experiments only being observed for materials that undergo interfacial sliding in the absence of significant plastic deformation and/or wear. In particular, the macroscale limits and temperature-independent friction coefficients can be thought of as energy dissipation through a host of opportunistic modes that are yet to be fully determined. The presence of such models significantly convolutes the *direct* interrogation of interfacial sliding forces in such system.

3.2. Graphitic systems

Thermally activated tribological behavior similar to that for polymer systems was observed in carbon nanotube systems

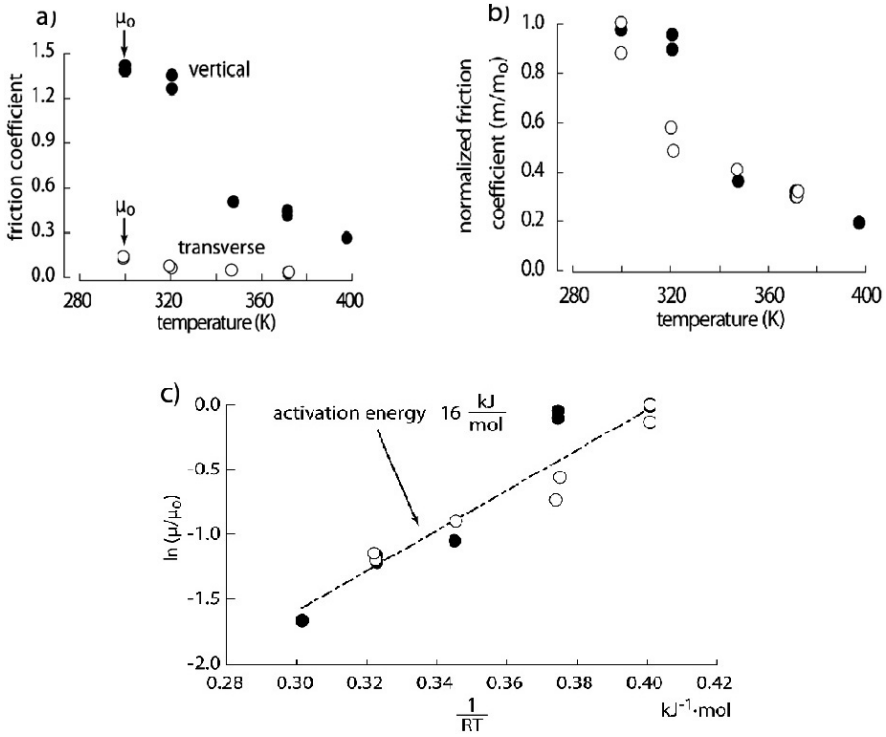

Figure 16. (a) Friction coefficient of multi-walled CNT films oriented in the transverse and vertical directions while sliding against a borosilicate glass lens. (b) The friction coefficients from (a) normalized by the value at 303 K. (c) An Arrhenius plot of the normalized friction coefficient with the activation energy indicated.

and the results are presented in figure 16 [33]. Figure 16(a) illustrates the friction coefficient of transversely and vertically oriented films of CNTs as a function of temperature during sliding against a borosilicate glass lens in an open air environment. There is a marked dependence of the friction coefficient on temperature in the case of the vertically aligned CNTs, whereas there is little change in friction coefficient with temperature in the case of the transversely aligned CNTs. However, figure 16(b), which illustrates the same friction coefficients normalized to the 303 K values, indicates that the relative change in friction coefficients over this temperature range are approximately the same for these two CNT films. An Arrhenius plot of the normalized friction, which is shown in figure 16(c), yields an activation energy of 16 kJ mol^{-1}, which is consistent with hydrogen bonding between the CNTs and the silica glass.

Variable-temperature friction results were also obtained on highly oriented pyrolytic graphite (HOPG) over a temperature range of 140–750 K, over which friction was observed to significantly increase at the lowest temperatures [54]. Briefly, an Omicron variable-temperature AFM (VT Beam Deflection AFM) with cooling and heating facilities provided access to friction measurements in a vacuum environment over a temperature range from 140 to 750 K. From 140 to 300 K, liquid nitrogen was used as a coolant while from 300 to 750 K, sample heating was achieved by a pyrolytic boron nitride heater mounted behind the sample. The HOPG sample was placed into the UHV chamber just after being cleaved. Before friction measurements, the HOPG sample was heated to 400 K until the background pressure recovered to its normal value. The base pressure in the UHV chamber is typically less than 2.0×10^{-10} Torr at room temperature.

The Si_3N_4 tips (Digital Instruments) used in the measurement had a cantilever normal force constant of $\sim$0.58 N m^{-1} and a nominal tip radius of $\sim$20 nm. Zero normal force was defined as being at the tip position where the cantilever was not bent. The scanning velocity in the experiments was fixed at 600 nm s^{-1} and the lateral scanning range was 100 nm. Friction measurements were performed as a function of increasing and decreasing load by control of the normal load through an external function generator. Reported friction coefficients were defined as the slope of the plot of friction versus load—an effectively linear response was observed under the low load conditions explored here.

Friction–load curves were measured over the temperature range 140–750 K. For room temperature and above, the friction data exhibited relatively little dependence on load. However, as the surface temperature was decreased, significant changes in the friction–load behavior were evident. From these data, coefficients of friction were recorded as the best-fit slopes to friction–load plots and normalized to the value measured at 300 K. The results are presented in figure 17. This temperature dependent data can be fit using the function

$$F \sim \exp(U_0/k_B T) \tag{3}$$

where U_0 is defined as a effective barrier to sliding. Analysis of the data provides a surface barrier U_0 is $\sim$10.8 kJ mol^{-1}. A barrier height for nanoscopic sliding on NaCl(100) has been reported as 0.25 eV at a normal load of 0.44 nN [57].

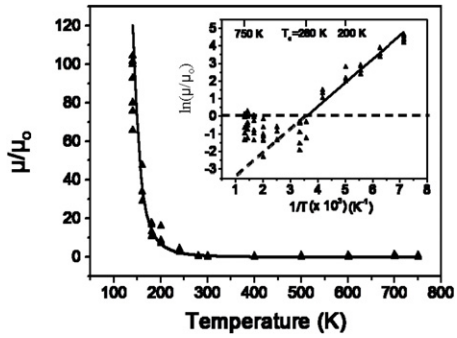

Figure 17. Normalized friction coefficients determined from friction–load behavior measured as a function of temperature for the contact of a Si_3N_4 probe tip sliding on HOPG as a function of temperature. Inset: an Arrhenius plot of the normalized friction coefficient data depict an activated sliding mechanism associated with energy dissipation process; very small values of friction values measured above 280 K result in deviations from an Arrhenius behavior. The fit to the experimental data corresponds to an activation barrier to sliding of 0.1 eV.

These measurements of interfacial friction, performed on the atomic scale for the contact of a microscopic probe tip and a single crystal surface, clearly portray a significant temperature dependence to the energy dissipated during sliding (friction). Specifically, a marked *increase* in friction is observed with *decreasing* surface temperature. It is important to note that every care has be taken to perform the measurements under controlled environments (ultrahigh vacuum) so as to avoid the potential contribution of adsorbates such as water, known to readily condense at cryogenic temperatures. In addition, the data have been collected for sliding events that, by and large, are not associated with any form of wear; wear at these length scales would constitute energetic events associated with bond breaking. This condition has been encouraged through the low force (pressure) measurements and verified through both the microscopic interrogation of the wear track (AFM imaging) as well as careful characterization of tip geometry before and after the extensive set of friction measurements.

Given the fundamental nature of the microscopic experiments and the high quality of the fit of the data to an exponential form, the data strongly suggest that the sliding events associated with frictional energy dissipation follow mechanisms entailing one or more activated steps. Furthermore, the data are seen to corroborate the temperature dependent friction behavior of the other materials described above for polymeric systems and to likewise suggest activated mechanisms of energy dissipation in those macroscopic systems as well. In terms of activated processes, the weak temperature dependence of friction for graphite observed above room temperature likely results from thermally induced motion of surface atoms and a blurring of local potentials responsible for the activated process at low temperatures.

4. Conclusions and future outlooks

The findings reviewed here indicate the power of combining computational and experimental methods across length and time scales. Materials in sliding contact involve the interplay between multiple chemical and physical processes, and it is unlikely that any single individual method or approach can fully determine all the relevant physical relationships. Rather, multidisciplinary approaches are needed to move the field forward. This is especially true for the combination of atomistic simulations, which directly probe the atomic processes that occur during sliding friction but are ultimately just predictions, with experimental data that provide only indirect evidence for phenomena but ultimately validate or disprove the computational predictions.

Do we need high performance computing and low contact pressure transfer-film experiments to tell us that stacks of 'Mikado-style' pick-up sticks will slide most easily along the axis of orientation? Probably not. But, how else will we develop the models and intuition that propels the field forward, and provide the opportunities to explore the details of composition, structural and molecular arrangement, and atomic-scale interfacial interactions that govern the complex phenomena of fundamental friction events? Together the molecular simulations and experiments challenge each other—pushing the fidelity, size, complexity, and sensitivities from opposite ends of time and length scale. Ultimately, the synergistic application of these tools will allow us to obtain the insights that will be necessary to prescribe and synthesize future, advanced tribological materials that can function at a superior level under a variety of extreme environments. Importantly, advances in the science of friction hold the potential to revolutionize many technologies through enhancements in energy efficiency, environmental impact, and lifetime of operation.

Acknowledgments

The authors gratefully acknowledge the contributions of their group members, including P R Barry, G R Bourne, D L Burris, P L Dickrell, M Hamilton, S-J Heo, I Jang, C Santos, and X Zhao, and the support of the US-AFOSR through MURI Grant No. FA9550-04-1-0367. They also thank the reviewer for valuable comments.

References

[1] Tomlinson G A 1929 A molecular theory of friction *Phil. Mag. Ser. 7* **7** 905–39
[2] Frenkel F C and Kontorova T 1938 On the theory of plastic demortation and twinning *Zh. Eksp. Teor. Fiz.* **8** 1340
[3] Dowson D 1979 *History of Tribology* (London: Longman)
[4] Johnson K L, Kendell K and Roberts A D 1971 Surface energy and the contact of elastic solids *Proc. R. Soc.* A **324** 301–13
[5] Perry S S 2004 Scanning probe microscopy measurements of friction *MRS Bull.* **29** 425–83
[6] Schmitz T, Action J, Ziegert J and Sawyer W G 2005 The difficulty of measuring low friction: uncertainty analysis for friction coefficient measurements *Tribol. Trans.* **127** 673–8
[7] Brenner D W, Shenderova O A, Harrison J A, Stuart S J, Ni B and Sinnott S B 2002 Second generation reactive empirical bond order (REBO) potential energy expression for hydrocarbons *J. Phys.: Condens. Matter* **14** 783–802

[8] Jang I and Sinnott S B 2004 Molecular dynamics simulations of the chemical modification of polystyrene through $C_xF_y^+$ beam deposition *J. Phys. Chem.* B **108** 9656–64

[9] Sinnott S B, Shenderova O A, White C T and Brenner D W 1998 Mechanical properties of nanotubule fibers and composites determined from theoretical calculations and simulations *Carbon* **36** 1–9

[10] Lennard-Jones J E 1931 Cohesion *Proc. Phys. Soc.* **43** 461–82

[11] Harrison J A, White C T, Colton R J and Brenner D W 1995 Investigation of the atomic-scale friction and energy-dissipation in diamond using molecular-dynamics *Thin Solid Films* **260** 205–11

[12] Perry M D and Harrison J A 1995 Universal aspects of the atomic-scale friction of diamond surfaces *J. Phys. Chem.* B **99** 9960–5

[13] Perry M D and Harrison J A 1996 Molecular dynamics investigations of the effects of debris molecules on the friction and wear of diamond *Thin Solid Films* **291** 211–5

[14] Gao G T, Mikulski P T and Harrison J A 2002 Molecular-scale tribology of amorphous carbon coatings: effects of film thickness, adhesion, and long-range interactions *J. Am. Chem. Soc.* **124** 7202–9

[15] Gao G T, Mikulski P T, Chateauneuf G M and Harrison J A 2003 The effects of film structure and surface hydrogen on the properties of amorphous carbon films *J. Phys. Chem.* B **107** 11082–90

[16] Garg A, Han J and Sinnott S B 1998 Interactions of carbon-nanotubule proximal probe tips with diamond and graphene *Phys. Rev. Lett.* **81** 2260–3

[17] Jang I, Sinnott S B, Danailov D and Keblinski P 2004 Molecular dynamics simulation study of carbon nanotube welding under electron beam irradiation *Nano Lett.* **4** 109–14

[18] Tutein A B, Stuart S J and Harrison J A 1999 Indentation analysis of linear-chain hydrocarbon monolayers anchored to diamond *J. Phys. Chem.* B **103** 11357–65

[19] Mikulski P T and Harrison J A 2001 Packing-density effects on the friction of *n*-alkane monolayers *J. Am. Chem. Soc.* **123** 6873–81

[20] Mikulski P T and Harrison J A 2001 Periodicities in the properties associated with the friction of model self-assembled monolayers *Tribol. Lett.* **10** 29–35

[21] Perry M D and Harrison J A 1997 Friction between diamond surfaces in the presence of small third-body molecules *J. Phys. Chem.* B **101** 1364–73

[22] Hu Y and Sinnott S B 2004 Molecular dynamics simulations of polyatomic-ion beam deposition induced chemical modification of carbon nanotube/polymer composites *J. Mater. Chem.* **14** 719–29

[23] Jang I and Sinnott S B 2004 Dependence of plasma-induced modification of polymer surfaces on polyatomic ion chemistry *Appl. Phys. Lett.* **84** 5118–20

[24] Hu Y, Shen S, Liu L, Wu S-Y, Jayanthi C and Sinnott S B 2002 Thin-film nucleation through molecular cluster beam deposition: comparison of tight-binding and many-body empirical potential molecular dynamics simulations *J. Chem. Phys.* **116** 6738–44

[25] Sinnott S B and Andrews R 2001 Carbon nanotubes: synthesis, properties and applications *Crit. Rev. Solid State Mater. Sci.* **26** 145–249

[26] Sinnott S B and Aluru N 2006 *Carbon Nanotechnology: Recent Developments in Chemistry, Physics, Materials Science and Device Applications* ed L Dai (Amsterdam: Elsevier) pp 361–488

[27] Ajayan P M, Schadler L S, Giannaris C and Rubio A 2000 Single-walled carbon nanotube-polymer composites: strengths and weaknesses *Adv. Mater.* **12** 750–3

[28] Falvo M R, Steele J, Taylor II R M and Superfine R 2000 Gearlike rolling motion mediated by commensurate contact: carbon nanotubes on HOPG *Phys. Rev.* B **62** R10664–7

[29] Falvo M R, Taylor R M, Helser A, Chi V, Brooks F P, Washburn S and Superfine R 1999 Nanomter-scale rolling and sliding of carbon nanotubes *Nature* **397** 236–8

[30] Schall J D and Brenner D W 2000 Molecular dynamics simulations of carbon nanotube rolling and sliding on graphite *Mol. Simul.* **25** 73–8

[31] Ni B and Sinnott S B 2001 Tribological properties of carbon nanotube bundles predicted from atomistic simulations *Surf. Sci.* **487** 87–96

[32] Dickrell P L, Sinnott S B, Hahn D W, Raravikar N R, Schadler L S, Ajayan P M and Sawyer W G 2005 Frictional anisotropy of oriented carbon nanotube surfaces *Tribol. Lett.* **18** 59–62

[33] Dickrell P L, Pal S K, Bourne G R, Muratore C, Voevodin A A, Ajayan P M, Schadler L S and Sawyer W G 2006 Tunable friction behavior of oriented carbon nanotube films *Tribol. Lett.* **24** 85–90

[34] Heo S-J, Sawyer W G, Perry S, Phillpot S R and Sinnott S B 2008 Effect of sliding orientation on the tribological properties of polyethylene in molecular dynamics simulations *J. Appl. Phys.* **103** 083502

[35] Smith B W, Russo R M, Chikkannanavar S B and Luzzi D E 2002 High-yield synthesis and one-dimensional structure of C_{60} encapsulated in single-wall carbon nanotubes *Nature* **396** 323–4

[36] Vasilev Y N, Yudin V P, Zlatkis A M and Kirichen V N 1972 *Dokl. Akad. Nauk SSSR* **203** 867

[37] Andoh Y, Oguchi S, Kaneko R and Miyamoto T 1992 Evaluation of very thin lubrication films *J. Phys. D: Appl. Phys.* **25** A71–5

[38] Mate C M 1995 Force microscopy studies of the molecular origins of friction and lubrication *IBM J. Res. Dev.* **39** 617–27

[39] Makinson K and Tabor D 1964 Friction and transfer of polytetrafluoroethylene *Nature* **201** 464–6

[40] Pooley C M and Tabor D 1972 Friction and molecular structure: the behavior of some thermoplastics *Proc. R. Soc.* A **329** 251–74

[41] Steijn R P 1968 Sliding experiments with polytetrafluoroethylene *ASLE Trans.* **11** 235–47

[42] Tanka K, Uchiyama Y and Toyooka S 1973 The mechanism of wear of polytetrafluoroethylene *Wear* **23** 153–72

[43] Blanchet T and Kennedy F 1992 Sliding wear mechanism of polytetrafluoroethylene (PTFE) and PTFE composites *Wear* **153** 229–43

[44] Pleskachevsky Y M and Smurugov V A 1997 Thermal fluctuations at PTFE friction and transfer *Wear* **209** 123–7

[45] Smurugov V, Senatrev A, Savkin V, Biran V and Sviridyonok A 1992 On PTFE transfer and thermoactivation mechanism of wear *Wear* **158** 61–9

[46] McLaren K and Tabor D 1963 Visco-elastic properties and the friction of solids: friction of polymers: influence of speed and temperature *Nature* **197** 856–8

[47] McCook N L, Burris D L, Dickrell P L and Sawyer W G 2005 Cryogenic friction behavior of PTFE based solid lubricant composites *Tribol. Lett.* **20** 109–13

[48] Breiby D W, Slling T I, Bunk O, Nyberg R B, Norrman K and Nielsen M M 2005 Structural surprises in friction-deposited films of poly(tetrafluoroethylene) *Macromolecules* **38** 2383–90

[49] Harrison J A, Stuart S J and Brenner D W 1999 *Handbook of Micro/Nanotribology* ed B Bhushan (Boca Raton, FL: CRC Press) pp 525–94

[50] Landman U, Luedtke W D and Gao J P 1996 Atomic-scale issues in tribology: interfacial junctions and nano-elastohydrodynamics *Langmuir* **12** 4514–28

[51] Jang I, Burris D L, Barry P L D P R, Santos C, Perry S S, Phillpot S R, Sinnott S B and Sawyer W G 2007 Sliding orientation effects on the tribological properties of polytetrafluoroethylene *J. Appl. Phys.* **102** 123509

[52] Gardos M N 1986 *Self-Lubricating Composites for Extreme Evnvironmental Conditions. Friction and Wear of Polymer Composites in the Composite Materials Series* ed K A P Friedrich (New York: Elsevier) pp 397–447
[53] Burris D L, Perry S S and Sawyer W G 2007 Macroscopic evidence of thermally activated friction *Tribol. Lett.* **27** 323–8
[54] Zhao X, Hamilton M, Sawyer W G and Perry S S 2007 Thermally activated friction *Tribol. Lett.* **27** 113–7
[55] Schirmeisen A, Jensen L, Hölscher H and Fuchs H 2006 Temperature dependence of point contact friction on silicon *Appl. Phys. Lett.* **88** 123108
[56] Sills S and Overney R M 2003 Creeping friction dynamics and molecular dissipation mechanisms in glassy polymers *Phys. Rev. Lett.* **91** 095501
[57] Gnecco E, Bennewitz R, Gyalog T, Loppacher C, Bammerlin M, Meyer E and Guntherodt H J 2000 Velocity dependence of atomic friction *Phys. Rev. Lett.* **84** 1172–5